Novel Hybrid Flow Diverter for Intracranial Aneurysm

Hao-Ming Hsiao (hmhsiao@ntu.edu.tw)
National Taiwan University
Ming-Ya Hung
National Taiwan University
Tzu-Yun Chou
National Taiwan University
Yu-Chieh Cheng
National Taiwan University
Li-Han Lin
National Taiwan University
Tzu-Yu Huang
National Taiwan University

Research Article

Keywords: Hemorrhagic Stroke, Intracranial Aneurysm, Hybrid Flow Diverter, Computational Fluid Dynamics, Advanced Medical Device.

Posted Date: August 2nd, 2021

DOI: https://doi.org/10.21203/rs.3.rs-730094/v1

Novel Hybrid Flow Diverter for Intracranial Aneurysm

Hao-Ming Hsiao*, Ming-Ya Hung, Tzu-Yun Chou, Yu-Chieh Cheng, Li-Han Lin, Tzu-Yu Huang

Department of Mechanical Engineering, National Taiwan University, Taipei, Taiwan

*Corresponding Author's E-mail: hmhsiao@ntu.edu.tw

Tel: 886-2-33669429

Abstract

An intracranial aneurysm is a weakened area in the wall of a cerebral artery which causes abnormal localized ballooning of the blood vessel. As an aneurysm grows, it puts pressure on adjacent structures and may eventually rupture, leading to severe complications or even sudden death. The standard treatments for intracranial aneurysms include traditional craniotomy and endovascular coiling. The purpose of these treatments is to stop the blood flow to an aneurysm to reduce the risk of rupture. In recent years, another new device, “flow diverter”, has gained popularity. It is placed in the parent artery to divert the blood flow away from the weakened area, isolating aneurysms from normal circulation. Although flow diverter stents have great potential, there remain clinical issues to be resolved.

This paper proposes a unique hybrid flow diverter, the first of its kind in the world, for treatment of the intracranial aneurysm. The hybrid flow diverter is designed to have variable mesh densities, with the denser side facing an aneurysm to block the blood flow and the lighter side facing the artery to prevent stenosis. It is deployed in the main cerebral artery next to an aneurysm to divert the blood flow away from the weakened aneurysm. Simulation results showed that the hybrid flow diverter reduced the blood flow into an aneurysm by a whopping 75–95%. The residence time of the blood flow inside an aneurysm was 12.47 times longer with the hybrid flow diverter, which may trigger thrombogenic reaction to fill an aneurysm and thus reduce the risk of rupture.

Keywords: Hemorrhagic Stroke, Intracranial Aneurysm, Hybrid Flow Diverter, Computational Fluid Dynamics, Advanced Medical Device.

1 Introduction

Cardiovascular disease (CVD), cancer, and stroke are the leading causes of death worldwide. Stroke can be divided into two main types: ischemic and hemorrhagic stroke. Hemorrhagic stroke may occur due to the spontaneous bursting of an intracranial aneurysm [1]. An intracranial aneurysm is a cerebrovascular disorder in which structural weakening of the wall media results in localized pathological dilation of the blood vessel. About 6% of the general population develop one or multiple intracranial aneurysms, which are relatively common in adults [2]. Patients harboring aneurysms are often unaware of their presence because most of these lesions are asymptomatic and small. The growth of aneurysms appears to be unpredictable and highly variable. As an aneurysm grows, it puts pressure on surrounding brain tissues and may eventually rupture, leading to fatal subarachnoid hemorrhage (SAH). SAH has high mortality, ranging from 25 to 50%, and causes severe disability in about 30% of survivors. Moreover, the rebleeding process may cause approximately 30% of untreated patients with intracranial aneurysms to die in the subsequent decade [3-4].

Treatment options for intracranial aneurysms generally include traditional craniotomy and endovascular coiling. In traditional craniotomy, an opening is made in the skull under general anesthesia, and a tiny clip is placed across the neck of an aneurysm to stop the blood flow into it. The purpose of surgical clipping is to isolate the aneurysm from the original circulation and thereby reduce the risk of rupture. Craniotomy has many limitations, such as the location, size, and geometry of the aneurysm, as well as the high possibility of complications induced by nerve damage and large aneurysms (larger than 25 mm) [5]. In addition, if the patient is old or in poor physical condition, the craniotomy is not recommended due to the high risks of invasion, the large wound, and the lengthy operation time.

Currently, a safer alternative to traditional craniotomy is a minimally invasive technique known as endovascular coiling. In this technique, an aneurysm is filled with coils to block it off from the main artery. The occlusive agent is a detachable platinum coil delivered through a micro-catheter positioned within an aneurysm. Although the success rate is high, limitations to the application of endovascular coiling treatment remain. One is the risk that the platinum coil may fall into the blood vessel and cause stroke when the aneurysmal neck diameter is greater than 4 mm or the aneurysmal dome to neck ratio is less than 2. In addition, although post-embolization angiography can show the degree of occlusion, the density of the coil packing cannot be adjusted, which may result in unstable and non-uniform strength. Also, if an aneurysm is not under equilibrium stress when the coils are inserted, it may cause the micro-catheter, guidewire, or coil to penetrate the aneurysm, leading to rupture and hemorrhage [6-9].

In recent years, another new device, the flow diverter, has been proposed to solve the problems mentioned above. The flow diverter is placed in the parent artery to divert blood flow away from the weakened area, isolating the aneurysm from the original circulation. Studies have shown that even for giant aneurysms with a high morbidity rate after endovascular coiling, deployment of a flow diverter has a high success rate for aneurysm sac embolization [10-11]. Although flow diverter stents have great potential, there remain clinical issues to be addressed. For example, excessively high metal coverage of the flow diverter may induce in-stent restenosis and block the parent artery, while low metal coverage may reduce the effect of flow diversion [12]. Also, the flow diverter should have advanced longitudinal flexibility to enter the brain, and its visibility also needs to be improved [13].

In this paper, a novel stent for interventional management of intracranial aneurysms, the hybrid flow diverter, is proposed. The hybrid flow diverter concept is

the first of its kind in the world. It was designed with variable metal densities such that the denser side faces an aneurysm to block the blood supply and the lighter side faces the parent artery to prevent in-stent restenosis. This provides a novel design to maintain the flow diverter performance of blocking blood flow and simultaneously reduce the clinical problems with comprehensive simulation verification.

2 Methodology

The development of the hybrid flow diverter is revealed, including the optimal design, finite element analysis of the manufacturing and deployment processes, and hemodynamic analysis before and after deployment. The parametric design methodology achieves the optimal design. Several finite element models were developed to analyze the structural integrity of the hybrid flow diverter during the manufacturing and deployment processes. The fatigue resistance of the device was evaluated by Goodman life analysis. Computational fluid dynamics models were established to assess the hemodynamic performance of the device. No human samples were involved in this study.

2.1 Hybrid Flow Diverter Design

2.1.1 Flow Diverter Basic Design

Flow diverters can be divided into two major types: laser-cut and braided metallic structures. The basic design of the laser-cut flow diverter was used as the standard stent in this study. A stent is an assembly of a series of cuddle rings interconnected with bridging links. The unit cell of a ring consists of a crown and a strut. A crown is a curved structure composed of two concentric arcs with different radii, and a strut is a straight portion connecting two adjacent crowns. A simple flow diverter, as

illustrated in Fig. 1, comprises several components: the strut width, ring spacing, crown radius, thickness, crown number, and ring number. These geometric parameters in different design patterns have critical impacts on the mechanical properties of flow diverters [14-15]. In this study, the mathematical relations between the different geometric parameters were established. Defining the relations between these parameters allowed quick modification of the parameters as needed and the automatic generation of new designs, which greatly improved the efficiency of design modification.

2.1.2 Hybrid Flow Diverter Design

The design pattern of a hybrid flow diverter is typically laser-cut directly onto a nitinol micro-hypotube. To avoid neointimal hyperplasia by high-profile metal, we propose a flow diverter with variable metal densities. The denser side faces an aneurysm to inhibit the blood flow, and the lighter side faces the parent artery to prevent in-stent restenosis. To make a flow diverter having a variety of metal densities, we defined the mathematical relations between different geometric parameters. For example, once the mesh density of the denser side (strut width, crown number and crown radius) was set, the crown radius of the lighter side could be automatically calculated for a fixed crown number and tube diameter.

In this study, a flow diverter was designed with different ring numbers, which strongly affect the strength of the denser and lighter sides. Due to the higher mesh density and greater ring number on the denser side, the crown expansion degree is relatively smaller, since the dense side is far stronger than the lighter side. On the other hand, the crown of the lighter side stretches to a great extent when expanding due to its low strength. Therefore, the design has to balance the strengths of the mesh

densities of the two sides.

Through adjustment of several designs and optimal parameters, a more balanced design of the mesh densities was found. Based on this design, the geometric model of the hybrid flow diverter proposed in this paper was constructed. Figs. 2a and 2b show the geometric structure of the hybrid flow diverter, which is mainly divided into four rings. The distal and proximal rings in the axial direction have low density, and the middle rings in the circumferential direction are divided into low and high density. The ring number ratio of the high vs. low density in the middle section is 2 to 1. Therefore, the denser side can block the blood flow to an aneurysm, and the lighter side, deployed in the parent artery, can avoid inducing neo-intimal hyperplasia at the same time.

2.2 Finite Element Analysis

In this paper, finite element analysis was conducted using the ABAQUS/Standard FEA solver (Dassault Systems Simulia Corp., Providence, RI, USA) with the user-defined UMAT subroutine [16]. The effects on the hybrid flow diverter in the manufacturing process were analyzed to confirm that the hybrid flow diverter could expand to the desired shape without material damage during manufacturing. After heat treatment and finalization, the hybrid flow diverter was further deployed in a model of an intracranial aneurysm to investigate its clinical behaviors. By obtaining the geometrical shape of the hybrid flow diverter deployed in the parent artery, we could ensure that no material damage would occur during the deployment process.

2.2.1 Material Properties

To make the hybrid flow diverter self-expand to its target shape and dimensions

in the parent artery, we used nitinol (NiTi) as the material due to its unique superelasticity and shape-memory properties. It is noted that, when force is applied, the austenite transforms into stress-induced martensite. After the load is removed, nitinol returns to its original shape due to the transformation between austenite and martensite. Since nitinol has more complex mechanical properties than ordinary metals, the hyperelastic properties of the ABAQUS finite element model needed to be set with the super-elastic user-defined material subroutine UMAT. The material used in this study was 2.0 mm nitinol hypotubes manufactured by the Minitube company. To make the material properties of the UMAT simulation closer to the actual material properties, we used the ABAQUS user plugin to correct the data repeatedly. It was found that the nitinol hypotube had about 12% elastic strain. When the strain caused by the load is less than 12%, then upon unloading, the material can recoil to its original shape. If the strain is more than 12% after the load is applied, the material is unable to revert to its original shape due to plastic deformation. Therefore, in this study, 12% strain was set as the safe upper limit to avoid the risk of material damage in the clinic.

2.2.2 Manufacturing Simulation

Several finite element models were developed to evaluate the structural integrity and pulsatile fatigue life of a hybrid flow diverter subjected to loading conditions consistent with current manufacturing and clinical practice [16-17]. These included hybrid flow diverter expansion and its corresponding heat treatment during manufacturing, crimping of the hybrid flow diverter inside a catheter for delivery, its release into a blood vessel, and pulsatile fatigue life under systolic/diastolic cycles relative to heart beats. The procedures were simulated in the following five major

steps:

Step 1: Expand the hybrid flow diverter to 4.0 mm ID.

Step 2: Heat treat the hybrid flow diverter after expansion.

Step 3: Crimp the hybrid flow diverter inside the 1.5 mm ID catheter for delivery.

Step 4: Release the hybrid flow diverter into the 4.0 mm ID blood vessel.

Step 5: Evaluate hybrid flow diverter pulsatile fatigue resistance under systolic/diastolic cycles by applying ± 3% stent diameter oscillation.

To simulate the hybrid flow diverter expansion during manufacturing and the crimping inside a catheter, two rigid cylindrical sleeves of different diameters were added to the model, with one inside the hybrid flow diverter and the other one outside the hybrid flow diverter [18]. During the expansion and subsequent heat treatment, the inner sleeve was expanded to the target size and the resulting stress/strain values in all elements of the FEA model were re-set to zero to simulate the stress relief process during heat treatment. After completion of the final expansion, the outer sleeve was applied to crimp the hybrid flow diverter inside the catheter for delivery. The third sleeve of 4 mm was then created to imitate the blood vessel. When the catheter was removed, the hybrid flow diverter sprang back until it contacted this 4 mm cylindrical surface.

Since the crowns of the hybrid flow diverter are subjected to high stresses/strains during expansion, the hybrid flow diverter was meshed with the incompatible mode 8-node brick element (C3D8I), which provides accurate predictions of maximum stress/strain with its integration points. On the other hand, two cylindrical sleeves were meshed with the three-dimensional, 4-node surface element with reduced integration (SFM3D4R). Because of the numerous contact interactions between surfaces in the simulation process, the function of the ABAQUS contact pair was

adopted to set the contacts, which were defined to prevent surface penetration [17]. In this study, both the contact pairs and the self-contact tangential friction coefficients were set to 0.1.

2.2.3 Fatigue Life Analysis

It is necessary for the hybrid flow diverter to withstand many types of stress and deformation when it is deployed in an artery, and the rhythmic pulsation of blood will present a major challenge to its fatigue resistance. If the structure cannot withstand extended periods of pulsation, the material may suffer fatigue damage and eventually fracture. The Food and Drug Administration (FDA) provides non-clinical engineering tests of intravascular stents and their associated delivery systems in the guidance document. FDA recommends that Goodman fatigue life analysis should be used to determine the fatigue safety factor under physiologic loading that simulates blood pressure conditions in the human body [19]. Following the simulations of stent manufacturing, a ± 3% stent diameter oscillation was applied to simulate pulsatile fatigue loading. The strain values of the integration points on the principal axis of the hybrid flow diverter obtained by finite element analysis were reprocessed to calculate the fatigue safety factor of the hybrid flow diverter, and then the fatigue resistance of the hybrid flow diverter was obtained. The results showed that fatigue failure would occur if the strain state in the device satisfied the following relation [16-17]:

$$\frac{\varepsilon_a}{\varepsilon_e} + \frac{\varepsilon_m}{\varepsilon_u} \geq 1 \tag{1}$$

where ε_a is the strain amplitude applied to the device, ε_e is the material endurance limit, ε_m is the mean strain applied to the device, and ε_u is the material ultimate strain. The Goodman diagram is a plot of the normalized strain amplitude $\varepsilon_a / \varepsilon_u$ (on

the y-axis) versus the normalized mean strain $\varepsilon_m / \varepsilon_u$ (on the x-axis). The equation $\varepsilon_a / \varepsilon_u + \varepsilon_m / \varepsilon_u = 1$ represents the failure line.

The fatigue safety factor (FSF) is defined as the ratio of the strain amplitude to the modified endurance limit. If the FSF is less than 1.0, it indicates that stent fatigue failure may take place due to pulsatile loading. If the FSF is greater than 1, it represents that the structure of the medical device is not prone to fatigue damage, and its fatigue resistance increases with increases in the FSF.

$$FSF = \frac{\varepsilon_e}{\varepsilon_a} \tag{2}$$

The position with the minimum FSF is the place where fatigue failure is most likely to occur. Therefore, the minimum FSF was used to evaluate the fatigue resistance of the hybrid flow diverter.

2.2.4 Stent-to-artery Ratio

One of the complications of treatment with flow diverters is the occurrence of in-stent stenosis due to its high metal coverage. Therefore, the hybrid flow diverter was designed with a higher area of coverage on the side facing the aneurysm and a lower area of coverage on the side facing the parent artery. The stent-to-artery ratio is considered an important clinical attribute, and it can be calculated using the following equation:

$$Stent-to-artery\ Ratio = \frac{A_{stent}}{A_{artery}} \tag{3}$$

where A_{stent} is the contact area between the outer surface of the hybrid flow diverter and the artery, and A_{artery} is the inner surface area of the artery.

2.2.5 Deployment Simulation in Intracranial Aneurysm Model

The heat-treated hybrid flow diverter was further deployed in the intracranial aneurysm model to obtain the steady-state results of the interaction between the hybrid flow diverter and the arterial wall. These results would indicate whether the hybrid flow diverter could be bent and deployed in the parent artery of an aneurysm. They could also be used to analyze whether material damage would occur during the deployment of the hybrid flow diverter. The procedures were simulated in the following three major steps:

Step 1: Crimp the hybrid flow diverter.

Step 2: Bend the hybrid flow diverter into the 4.0 mm ID parent artery.

Step 3: Release the hybrid flow diverter, and the deployment is completed.

The deployment models included the vascular geometry model of an intracranial aneurysm, the hybrid flow diverter after heat treatment, and the cylindrical sleeve to crimp the hybrid flow diverter and assist deployment. The ABAQUS VDISP subroutine was used to control the displacement of the nodes on the cylindrical sleeve with the hybrid flow diverter inside such that the centerline of the sleeve would overlap with the centerline of the parent artery, and the hybrid flow diverter was bent to the parent artery for deployment.

We referred to the ideal intracranial aneurysm geometry proposed by Wu et al. and the vascular thickness presented by Sanchez et al. [20-21]. Fig. 3a illustrates the intracranial aneurysm model. It can be mainly divided into two parts: an aneurysm and the parent artery. In the intracranial aneurysm model, an aneurysm is a hollow ball with a lumen diameter of 5.2 mm and thickness of 0.38 mm; the parent artery is a long curved tube with a lumen diameter of 4.0 mm, thickness of 0.6 mm, length of 30.0 mm, and bending angle of 120 degrees. Given the different natures of the

materials, an aneurysm being delicate and soft while the parent artery is tough, different material parameters were applied respectively. The material of an aneurysm can be found in the study of Costalat et al., which classified the material properties of an aneurysm into hard, medium, and soft, and the three levels of the corresponding risk of aneurysm rupture as low, medium and high [22-23]. We used the hierarchy of soft as the material property of an aneurysm. The Mooney–Rivlin model was adopted to construct the material of the aneurysm, while the parent artery was constructed with reference to the second order hyperelastic constitutive model proposed by Creane et al. [24]. The materials of the arterial wall were assumed to be hyperelastic, homogeneous, isotropic and incompressible. The strain energy potential of the two materials can be defined as follows:

$$W_s = C_{10}\left(I_1 - 3\right) + C_{01}\left(I_2 - 3\right) + C_{11}\left(I_1 - 3\right)\left(I_2 - 3\right) \tag{4}$$

$$\begin{aligned} W_p = {} & C_{10}\left(I_1 - 3\right) + C_{01}\left(I_2 - 3\right) + C_{11}\left(I_1 - 3\right)\left(I_2 - 3\right) \\ & + C_{20}\left(I_1 - 3\right)^2 + C_{02}\left(I_2 - 3\right)^2 \end{aligned} \tag{5}$$

where W_s is the strain energy potential of the aneurysm, W_p is the strain energy potential of the parent artery, I_1 is first deviatoric strain invariants, I_2 is second deviatoric strain invariants, and C_{10}, C_{01}, C_{11}, C_{20} and C_{02} are material parameters, which are shown in Table 1.

For the intracranial aneurysm model, the sweep method can be used to generate hexahedron meshes after proper geometric partitioning, so it was meshed with an 8-node hexagonal element with reduced integration (C3D8RH). The 4.0 mm ID hybrid flow diverter after heat treatment was adopted in the deployment simulation. The element types of the hybrid flow diverter and the cylindrical sleeve were meshed with the same method in the manufacturing simulation.

2.3 Computational Fluid Dynamics

In this study, the blood flow model of an intracranial aneurysm was used for hemodynamic analysis to evaluate the capability of the hybrid flow diverter to block the blood flow and to analyse the wall shear stress before and after the deployment. After the manufacturing and deployment simulation, the hybrid flow diverter was further used to establish a hemodynamic model to analyse the clinical behaviour of the hybrid flow diverter.

2.3.1 Material Properties

Blood usually behaves like a Newtonian fluid when the shear rate is greater than 100 s^{-1} [25]. However, due to flow disturbances, the actual shear rates in stented arteries could become lower than 100 s^{-1}. Therefore, in this paper, blood flow was assumed to be steady, non-Newtonian, incompressible, and laminar. The effects of other components in the blood, such as cells, proteins, ions, nutrients, and excreta, were not considered. Since the range of human body temperature changes is not obvious, the influence of temperature on blood was not taken into account.

Due to the low Reynolds number of blood, it was input as a laminar fluid with a density of 1060 kg/m^3 [26]. The Carreau model was used to describe the non-Newtonian characteristics of the blood and is given in Eq. (6):

$$\mu = \mu_\infty + \left(\mu_0 - \mu_\infty\right)\left[1+\left(\lambda\dot{\gamma}\right)^2\right]^{\frac{n-1}{2}} \tag{6}$$

where μ_∞ and μ_0 are the viscosities when the shear rate approaches infinity and zero, respectively, λ and n are the material coefficients, and γ is the shear rate. These parameters were obtained by curve-fitting the Carreau model to the experimental data found in the literature, and their values were $\mu_\infty = 0.0035$ kg/m-s,

$\mu_0 = 0.25$ kg/m-s, $\lambda = 25.0$ s, and $n = 0.25$ [27-28]. Fig. 3b plots the relation between dynamic viscosity and shear strain rate based on the above parameters for the Carreau–Yasuda Model.

2.3.2 Governing Equations

In this study, the blood flow was assumed to be an incompressible, single phase and laminar flow with no impact of temperature. Therefore, only fluid mass and momentum conversation were considered, and the governing equations are the conservation laws of mass and momentum, given in Eqs. (7) and (8), respectively:

$$\nabla \cdot v = 0 \tag{7}$$

$$\rho\left(\frac{\partial v}{\partial t} + v \cdot \nabla v\right) = -\nabla p + \nabla \cdot \tau_{ij} \tag{8}$$

where v is velocity, ρ is density, p is pressure, and τ_{ij} is shear stress, which is viscosity μ times shear strain rate γ :

$$\tau_{ij} = \mu\dot{\gamma}_{ij} = \mu\left(\frac{dv_i}{dx_j} + \frac{dv_j}{dx_i}\right) \tag{9}$$

Simulations were conducted by using the CFD solver FLUENT (ANSYS, Inc., Canonsburg, PA, USA) with a finite-volume method. The flow equations were discretized for each cell in the model. The pressure–velocity coupled algorithm, capable of solving velocity and pressure fields simultaneously, was used to provide robust solutions.

2.3.3 Womersley Flow

Blood flow is a pulsatile flow with periodic variations, so we adopted the analytic solutions of periodic Newtonian fully developed flow proposed by Womersley as the boundary condition of the inlet [29]. The analytic solutions of fully-developed flow

proposed by Womersley describe a homogeneous, incompressible and Newtonian fluid in a long straight pipe within the periodic oscillation of the analytic solution of the Navier-Stokes equations, assuming that the arterial wall is a round and rigid body and that the movement of fluid is in axial symmetry along the arterial wall, and not considering the radial components of the fluid. The axial velocity of blood flow can be defined as follows:

$$v_z(r,t) = \mathrm{Re}\left[\overline{v} \cdot \frac{1 - \dfrac{J_0\left(\alpha j^{\frac{3}{2}} y\right)}{J_0\left(\alpha j^{\frac{3}{2}}\right)}}{1 - \dfrac{2J_1\left(\alpha j^{\frac{3}{2}}\right)}{\alpha j^{\frac{3}{2}} J_0\left(\alpha j^{\frac{3}{2}}\right)}} \cdot e^{j\omega t} \right] \tag{10}$$

where v_z is the axial flow velocity, Re [ ] means taking the real part, $\overline{v} = \dfrac{Q}{\pi R^2}$ is the average flow velocity of the cross section, J_0 ( ) and J_1 ( ) are the Bessel functions of the first kind of zero order and the first order respectively, α is the Womersley constant, $j = \sqrt{-1}$, and ω is the oscillation frequency. Since $\overline{v}$ is composed of periodic functions, a Womersley flow whose inlet velocity varies with any period can be decomposed into $\overline{v} = \sum_{i=1}^{n} \overline{v}_i$ with $n \in N^+$ by Fourier series. Therefore, various inlet boundary conditions can be fitted.

2.3.4 Hemodynamic Models and Boundary Conditions

Simulation results obtained from the finite element analysis were further applied to the computational fluid dynamics simulation through reverse engineering. The flow field model of an intracranial aneurysm in this study was an ideal intracranial

aneurysm model proposed by Xu et al. [20]. The geometric shape of an aneurysm was a sphere with a diameter of 5.2 mm, and the connected parent artery had a diameter of 4.0 mm, length of 30.0 mm, and bending angle of 120 degrees. Blood flowed into the artery via the lower entrance. The flow field model of an intracranial aneurysm after deployment of the hybrid flow diverter is shown in Figs. 4a and 4b.

In this paper, the arterial wall was assumed to be a fixed, no-slip surface, and the hybrid flow diverter was also assumed to be a rigid body fixed on the arterial wall. The inlet and outlet boundary conditions are shown in Figs. 4a and 4b. The inlet boundary condition was the inlet pulsatile velocity waveform for blood flow in the study by Xu et al., which was obtained by calculating the average inlet pulsatile velocity for blood flow in healthy subjects through Transcranial Doppler (TCD). The average flow velocity used in this paper is shown in Fig. 4c. Constant pressure was applied for the boundary condition in the outlet, while the pressure value in the outlet was fixed at 1 atmosphere. We assumed that blood was a non-Newtonian fluid, but Womersley flow adopted the assumption that the fluid was a Newtonian fluid. Therefore, to apply boundary conditions at the inlet as the velocity profile of Womersley flow shown in Fig. 4c, it was necessary to confirm initially whether the viscosity coefficient could be regarded as a Newtonian fluid at the inlet. It can be seen from Fig. 3b that when the shear strain rate is greater than 100 s^{-1}, the viscosity gradually tends toward a constant value. At this point, the fluid can be regarded as a Newtonian fluid, and the viscosity is $\mu_\infty = 0.0035\,\text{kg/m-s}$.

The flow field model of an intracranial aneurysm after the hybrid flow diverter deployment was simulated in the transient state using the analytic solution of inlet pulsatile flow of the aforementioned Womersley flow. The pulsatile period was divided into 80 time steps of 0.01 seconds each. To ensure the stability of the solution,

the simulation results of the third period, namely 1.6–2.4 seconds, were taken in this study. The hemodynamic model was simulated in ANSYS FLUENT, with the user-defined function (UDF) to provide a variety of advanced solving functions. The boundary conditions of Womersley flow were set by the user-defined function.

The blood dynamics model of an intracranial aneurysm was meshed with the tetrahedron elements. Because the no-slip arterial wall boundary conditions would make the gradient change in physical quantities greater in the direction of the vertical wall than in that of the parallel wall, the dynamics model near the arterial wall, the part of the hybrid flow diverter deployment, and the aneurysm neck were meshed in densely to capture the physical quantities with a large gradient change for accuracy.

2.3.5 Observation Indicators

To predict the clinical behaviours of the hybrid flow diverter, the blood inflow and inflow velocity of an aneurysm, residence time, and wall shear stress were used as observation indicators in this study. The stability of the flow within an aneurysm, such as the blood flow rate or flow into an aneurysm, has been used in many studies to assess the risk of aneurysm rupture [30-31]. In this study, the blood flow velocity inside the aneurysm was analysed and the blood flow into the aneurysm was measured to assess the stability of the flow inside the aneurysm. In the flow field model of the intracranial aneurysm, the plane with a normal vector toward the inside of the aneurysm was set to monitor blood flow (Fig. 5a). The net blood flow through the plane was the sum of inflow and outflow:

$$Q_{net} = Q_{in} + Q_{out} \tag{11}$$

where Q_{net} is the net blood flow, Q_{in} is the net blood inflow, and Q_{out} is the net blood outflow through the plane. The blood flow into an aneurysm can be obtained by

calculating the dot product of the blood inflow velocity through the plane with the normal vector of the plane:

$$Q_{in} = \int \vec{V}_{in} \cdot d\vec{A} = \int \vec{V}_{in} \cdot \vec{n} dA \tag{12}$$

where $\vec{n}$ is the unit normal vector of the plane, A is the area of the plane that intersects an aneurysm, and $\vec{V}_{in}$ is the blood inflow velocity through the plane, which can be obtained by the Heaviside step function.

Janiga et al. proposed the parameter of residence time [32], which can evaluate the influences of different aneurysm geometries, as defined below:

$$t_r = \frac{V_{AS}}{Q_{in}} \tag{13}$$

where t_r is residence time, Q_{in} is the inflow of the aneurysm, and V_{AS} is the volume of the aneurysm. The residence time represents the stability of blood flow within an aneurysm. The greater the residence time, the more stable the blood is, and thus the lower the risk of aneurysm rupture. Since the residence time considers the factor of aneurysm volume, differences in residence time can be compared even for aneurysms of different volumes.

After stenting, neo-intimal hyperplasia and thus restenosis occur in some patients. Clinical results have shown that low wall shear stress or oscillating wall shear stress corresponds to the occurrence of the greatest neo-intimal hyperplasia in stented arteries [33-34]. Moreover, excessively high or low wall shear can induce neo-intimal hyperplasia, so wall shear stress has been seen as an important indictor to predict the potential risk of restenosis. In FLUENT, the definition of vascular wall shear stress is as follows:

$$\tau_w = \mu \left(\frac{\partial v}{\partial n} \right) \tag{14}$$

where v is the blood flow velocity, and n is the normal vector to the arterial wall. In

this paper, the absolute value of shear stress $|\tau_w|$ is used as the observation indicator.

In addition, an intracranial aneurysm in an area of low flow velocity and low wall shear stress can easily lead to platelet thrombosis [35]. Some studies have also shown that high wall shear stress increases the risk of aneurysm rupture, so blood flow in an aneurysm with low wall shear stress is relatively favourable [36-38]. It has been suggested that shear stress of less than 5 dynes/cm^2 leads to endothelial proliferation of smooth muscle cells [39], so the size of the low wall shear area (that is, the area of wall shear stress less than 5 dynes/cm^2) on the arterial wall was also an important observation indicator.

3 Results and Discussion

3.1 Finite Element Analysis

3.1.1 Manufacturing Simulation

Figs. 6a and 6b show the strain distribution of the hybrid flow diverter when it was expanded to 4.0 mm ID and crimped to 1.5 mm OD. After the expansion, the balance between metal densities and feasibility was successfully achieved by the parametric design. The hybrid flow diverter could both prevent blood from flowing into an aneurysm and avoid stimulating the growth of the endothelial cells of the parent artery at the same time. Icon SDV24 (solution-dependent state variable 24) is the variable name in ABAQUS UMAT. In the hyperelastic material of UMAT, SDV24 represents variables for the equivalent elastic strain. As shown in Fig. 6a and 6b, in the process of either expansion or crimping, the regions near the crown indicated higher strain energy, while it was relatively low in the parts near the struts. The strain levels were 1.37% and 1.70% when the hybrid flow diverter was expanded to 4.0 mm ID and crimped to 1.5 mm OD, respectively. In addition, in both steps, the elastic strain of the

nitinol material was kept within 12%. Thus, it was below the upper limit of safe working strain, indicating that the material of the hybrid flow diverter would not be damaged during the manufacturing process.

3.1.2 Fatigue Life Analysis

According to the simulation results, Goodman fatigue life analysis defined fatigue safety factors of the hybrid flow diverter in terms of normalized mean strain and strain amplitude (Fig. 6c). The blue data points in the figure are the distribution of each integration point on the hybrid flow diverter by mean strain values and strain amplitude values. Since the fatigue safety factor represented the position with the worst fatigue resistance capability, the blue data point closer to the Goodman diagram failure line revealed the smaller fatigue safety factor. The results showed that the calculated points fell far below the Goodman diagram failure line and indicated excellent fatigue resistance. The fatigue safety factor was 5.63, which met the requirements of fatigue safety.

3.1.3 Stent-to-Artery Ratio

A hybrid flow diverter with various metal densities is proposed in this paper to achieve different stent-to-artery ratios. Fig. 6d compares the metal densities from the lighter side to the denser side of the hybrid flow diverter after expansion. The different metal densities entailed dissimilar artery area coverages, and the stent-to-artery ratios were 19.58% and 10.42% for the sides facing the aneurysm and the parent artery, respectively. Therefore, the hybrid flow diverter indeed blocked the blood flow into an aneurysm with relatively high metal coverage and avoided excessive contact with the parent artery on the lighter side.

3.1.4 Deployment Simulation

Fig. 5c presents the simulation results of the hybrid flow diverter deployment. When the hybrid flow diverter moved with the bending cylindrical sleeve and the centerline overlapped with the parent artery, the maximum strain value was 1.19%, which was still within the safe strain range of the nitinol material. The strain gradually decreased to 0.84% as the hybrid flow diverter was released in the parent artery. Therefore, no material damage would take place during the deployment process. Fig. 5c also shows the final result of the hybrid flow diverter deployment to the parent artery.

3.2 Computational Fluid Dynamics

3.2.1 Inflow Rate

Fig. 5b plots the inflow ratio of the surface monitor and inlet boundary before deployment of the hybrid blood diverter. The calculated results showed that the blood volume in the aneurysm accounted for about 3–6% of the blood volume at the inlet boundary. Fig. 7a plots the inflow rate measured by the surface monitor before and after deployment of the hybrid flow diverter, respectively. After deployment, the blood flow into the aneurysm was significantly reduced, by 75–95%. As shown in Fig. 7b, the hybrid flow diverter prevented most of the blood from flowing into the aneurysm.

3.2.2 Residence Time

The results on the residence time showed that the hybrid flow diverter significantly increased it (Fig. 8a). The original residence time range before the deployment was 0.08–0.20 seconds. After deployment of the hybrid flow diverter, the

residence time improved to 0.34–4.23 seconds. The average residence time had a whopping increase from 0.15 seconds to 1.87 seconds, an increase of 12.47 times. The increases in residence time after deployment shown in Fig. 8b revealed that the maximum and minimum residence time increased by 0.79 seconds and 0.10 seconds, respectively. The simulation results showed that the hybrid flow diverter significantly increased the residence time, which may trigger thrombogenic reaction to fill an aneurysm and thus reduce the risk of aneurysm rupture.

3.2.3 Velocity Distribution

Since the maximum increase in the residence time was 0.79 seconds, that time was used to present the streamline and the contour of flow velocity for an intracranial aneurysm. Fig. 9a presents the contour plots of comparison for the streamline before and after the deployment of the hybrid flow diverter. The streamline indicated that the hybrid flow diverter successfully blocked the blood flow into the aneurysm, and only a small amount of blood entered the aneurysm through the hollows. As shown in the partial enlargement of the streamline in Fig. 9b, the blood flow into the aneurysm was substantially reduced. Fig. 10a shows the central section of the flow velocity contour before and after the deployment of the hybrid flow diverter. From the partial enlargement of the flow velocity shown in Fig. 10b, it is clear that the blood flow rate inside the aneurysm decreased sharply after the deployment, and the aneurysm also maintained a stable blood flow inside it. Therefore, the hybrid flow diverter effectively blocked the blood flow into the aneurysm.

3.2.4 Wall Shear Stress distribution

Since the maximum increase in residence time was 0.79 seconds, that time was

also used to present the contour of wall shear stress distribution for an intracranial aneurysm. Fig. 11a shows the wall shear stress distribution before and after the deployment of the hybrid flow diverter. Due to the faster flow velocity in the aneurysm before the deployment of the hybrid flow diverter, only a few areas in the aneurysm had low shear stress (< 5 dynes/cm^2). After the deployment of the hybrid flow diverter, the reduced blood flow into the aneurysm was accompanied by a decrease in the blood flow rate, so the wall shear stress of the aneurysm also fell sharply, to mostly less than 5 dynes/cm^2. As an area of low flow rate and low wall shear stress is prone to thrombosis due to platelet aggregation, an aneurysm would eventually heal as the thrombus filled up the entire lumen over time. According to some studies, higher wall shear stress will increase the risk of aneurysm rupture. Therefore, the hybrid flow diverter not only reduced the wall shear stress of the aneurysm but also alleviated the risk of aneurysm rupture.

Fig. 11b shows a partial enlargement of the wall shear stress distribution contour after the deployment of the hybrid flow diverter. In the parent artery, the region near the crowns of the hybrid flow diverter had a low wall shear stress distribution. This phenomenon was the same as those in previous studies, which indicated that the reduced wall shear stress promoted endothelial cell proliferation, thus resulting in stenosis. Therefore, to avoid neo-intimal hyperplasia of the parent artery due to high metal coverage, the hybrid flow diverter was designed with a lower crown number on the side facing the parent artery so that the area of low wall shear stress could be reduced and excessive endothelial cell proliferation could be prevented.

4 Conclusions

A novel design concept of the flow diverter is proposed to address potential clinical problems. The hybrid flow diverter is designed with variable metal densities to both block the blood supply with the denser side facing an aneurysm and prevent in-stent restenosis with the lighter side facing the parent artery. To construct and evaluate such a hybrid flow diverter, optimal design, FEA simulation, and CFD simulation were applied. Through the parametric design methodology, we achieved optimization of the hybrid flow diverter. FEA simulation results of the optimized hybrid flow diverter showed no material damage occurring during the manufacturing and deployment process because the strain was within the safety range. Also, the calculated fatigue safety factor was 5.629, which met the standard. CFD simulation results showed that the hybrid flow diverter stopped 75–95 percent of the blood flow into an aneurysm. The average blood flow residence time within an aneurysm increased by 12.47 times, so the stasis was elongated and thrombogenic conditions were produced. In addition, the stable blood flow also significantly reduced the risk of aneurysm rupture. Wall shear stress in the aneurysm sac also dropped significantly after deployment of the flow diverter, while low wall shear stress area in the parent artery decreased due to the lighter metal density, thus preventing in-stent thrombosis or restenosis. These conclusions suggest that the hybrid flow diverter allows complete reconstruction of the diseased segment of an intracranial artery and has great implications for future design optimization to achieve the best possible clinical outcomes.

Acknowledgement

This research was sponsored by the Ministry of Science and Technology through Grants MOST-110-2622-E-002-028 and MOST-108-2221-E-002-153-MY3. The authors gratefully appreciate the support and help from MOST.

References

[1] E. S. Jr. Connolly, A. A. Rabinstein, J. R. Carhuapoma, *et al*, "Guidelines for the management of aneurysmal subarachnoid hemorrhage: a guideline for healthcare professionals from the American Heart Association/American Stroke Association," *Stroke,* vol. 43, pp. 1711-1737, 2012.

[2] G. J. Rinkel, M. Djibuti, A. Algra, *et al*, "Prevalence and risk of rupture of intracranial aneurysms a systematic review," *Stroke,* vol. 29, pp. 251-256, 1998.

[3] G. J. Rinkel, M. Djibuti, A. Algra, *et al*, "Prevalence and risk of rupture of intracranial aneurysms a systematic review," *Stroke,* vol. 29, pp. 251-256, 1998

[4] J. L. Brisman, J. K. Song, and D. W. Newell, "Cerebral aneurysms," *New England Journal of Medicine,* vol. 355, pp. 928-939, 2006.

[5] R. A. Solomon, M. E. Fink, and J. Pile-Spellman, "Surgical management of unruptured intracranial aneurysms," *Journal of Neurosurgery,* vol. 80, pp. 440-446, 1994.

[6] A. F. Zubillaga, G. Guglielmi, F. Vinuela, *et al*, "Endovascular occlusion of intracranial aneurysms with electrically detachable coils: correlation of aneurysm neck size and treatment results," *American Journal of Neuroradiology,* vol. 15, pp. 815-820, 1994.

[7] H. Dinç, M. H. Öztürk, A. Sari, et al, "Coil embolization in 481 ruptured intracranial aneurysms: angiographic and clinical results," *Diagnostic and*

Interventional Radiology, vol. 19, p. 165, 2013.

[8] G. M. Debrun, V. A. Aletich, P. Kehrli, *et al*, "Selection of cerebral aneurysms for treatment using Guglielmi detachable coils: the preliminary University of Illinois at Chicago experience," *Neurosurgery*, vol. 43, pp. 1281–1295, 1998.

[9] G. M. Debrun, V. A. Aletich, P. Kehrli, *et al*, "Aneurysm geometry: an important criterion in selecting patients for Guglielmi detachable coiling," *Neurol Med Chir (Tokyo)*, vol. 38, pp. 1–20, 1998.

[10] D. Fiorella, F. C. Albuquerque, V. R. Deshmukh, *et al*, "Usefulness of the Neuroform stent for the treatment of cerebral aneurysms: results at initial (3–6 mo) follow-up," *Neurosurgery*, vol. 56, pp. 1191–1201, 2005.

[11] D. Fiorella, P. Lylyk, I. Szikora, *et al*, "Curative cerebrovascular reconstruction with the Pipeline embolization device: the emergence of definitive endovascular therapy for intracranial aneurysms," *J Neurointervent Surg*, vol. 1, pp. 56–65, 2009.

[12] Y. J. Alderazi, D. Shastri, T. Kass-Hout, et al, "Flow diverters for intracranial aneurysms," *Stroke Research and Treatment*, vol. 2014, Article ID 415653, 2014.

[13] T. Watson, M. W. I. Webster, J. A. Ormiston, *et al*, "Long and short of optimal stent design," *Open Heart*, vol. 4, e000680, 2017.

[14] H. M. Hsiao, Y. H. Chiu, K. H. Lee, *et al*, "Computational modeling of effects of intravascular stent design on key mechanical and hemodynamic behavior," *Computer-Aided Design,* vol. 44, pp. 757-765, 2012.

[15] H. M. Hsiao, K. H. Lee, Y. C. Liao, *et al*, "Cardiovascular stent design and wall shear stress distribution in coronary stented arteries," *Micro & Nano Letters*, vol. 7, pp. 430-433, 2012.

[16] H. M. Hsiao, L. W. Wu, and M. T. Yin et al, “Quintupling fatigue resistance of intravascular stents via a simple design concept.” *Computational Materials Science*,

vol. 86, pp. 57–63, 2014.

[17] H. M. Hsiao, C. H. Lin, and Y. K. Shen et al., “Rhombic-shaped channel stent with enhanced drug capacity and fatigue life,” *Micromachines*, vol. 9(1):3, 2018.

[18] H. M. Hsiao, Y. Y. Wu, and B. C. Tsai et al. “Investigation of fibrous cap stresses on vulnerable plaques leading to heart attacks,” *Technology and Health Care*, vol. 24 (s1), pp. S155–S161, 2016.

[19] U. F. a. D. Administration, "Non-clinical engineering tests and recommended labeling for intravascular stents and associated delivery systems," 2010.

[20] J. Xu, Z. Wu, Y. Yu, *et al*, "Combined effects of flow diverting strategies and parent artery curvature on aneurysmal hemodynamics: A CFD Study," *PLoS One,* vol. 10, p. e0138648, 2015.

[21] M. Sanchez, D. Ambard, V. Costalat, *et al*, "Biomechanical assessment of the individual risk of rupture of cerebral aneurysms: a proof of concept," *Annals of Biomedical Engineering,* vol. 41, pp. 28-40, 2013.

[22] V. Costalat, M. Sanchez, D. Ambard, *et al*, "Biomechanical wall properties of human intracranial aneurysms resected following surgical clipping (IRRAs Project)," *Journal of Biomechanics,* vol. 44, pp. 2685-2691, 2011.

[23] M. Sanchez, O. Ecker, D. Ambard, *et al*, "Intracranial aneurysmal pulsatility as a new individual criterion for rupture risk evaluation: biomechanical and numeric approach (IRRAs Project)," *AJNR Am J Neuroradiol,* vol. 35, pp. 1765-1771, 2014.

[24] A. Creane, E. Maher, S. Sultan, *et al*, "Finite element modelling of diseased carotid bifurcations generated from in vivo computerised tomographic angiography," *Computers in Biology and Medicine,* vol. 40, pp. 419-429, 2010.

[25] D.N. Ku, D.P. Giddens, et al. "Pulsatile flow and atherosclerosis in the human carotid bifurcation. Positive correlation between plaque location and low oscillating

shear stress," *Arteriosclerosis: An Official Journal of the American Heart Association*, pp. 293-302, 1985.

[26] J. D. Cutnell and K. W. Johnson, "Physics. 4th Edition," ed: John Wiley & Sons Ltd., New York, 1998.

[27] S. Chien, S. Usami, H. M. Taylor, *et al*, "Effects of hematocrit and plasma proteins on human blood rheology at low shear rates," *Journal of Applied Physiology,* vol. 21, pp. 81-87, 1966.

[28] T. Seo, L. G. Schachter, and A. I. Barakat, "Computational study of fluid mechanical disturbance induced by endovascular stents," *Ann Biomed Eng*, vol.33, pp. 444-456, 2005.

[29] J. R. Womersley, "Method for the calculation of velocity, rate of flow and viscous drag in arteries when the pressure gradient is known," *The Journal of Physiology,* vol. 127, p. 553, 1955.

[30] W. Fu, Z. Gu, X. Meng, *et al*, "Numerical simulation of hemodynamics in stented internal carotid aneurysm based on patient-specific model," *Journal of Biomechanics,* vol. 43, pp. 1337-1342, 2010.

[31] P. K. Nelson, P. Lylyk, I. Szikora, *et al*, "The pipeline embolization device for the intracranial treatment of aneurysms trial," *American Journal of Neuroradiology,* vol. 32, pp. 34-40, 2011.

[32] G. Janiga, C. Rössl, M. Skalej, and D. Thévenin, "Realistic virtual intracranial stenting and computational fluid dynamics for treatment analysis," *Journal of Biomechanics,* vol. 46, pp. 7-12, 2013.

[33] D. C. Chappell, S. E. Varner, R. M. Nerem, *et al*, "Oscillatory shear stress stimulates adhesion molecule expression in cultured human endothelium," *Circ Res*, vol. 82, pp. 532-539, 1998.

[34] D. N. Ku, C. K. Zarins, D. P. Giddens, *et al*, "Pulsatile flow and atherosclerosis in the human carotid bifurcation: positive correlation between plaque localization and low and oscillating shear stress," *Arteriosclerosis*, vol. 5, pp. 292-302, 1985.

[35] V. L. Rayz, L. Boussel, M. T. Lawton, *et al*, "Numerical modeling of the flow in intracranial aneurysms: prediction of regions prone to thrombus formation," *Ann Biomed Eng*, vol. 36, pp. 1793-1804, 2008.

[36] K. Kataoka, M. Taneda, T. Asai, *et al*, "Structural fragility and inflammatory response of ruptured cerebral aneurysms: a comparative study between ruptured and unruptured cerebral aneurysms," *Stroke*, vol. 30, pp. 1396-1401, 1999.

[37] Y. Qian, H. Takao, K. Fukui, *et al*, "Computational risk parameter analysis and geometric estimation for cerebral aneurysm growth and rupture," *Stroke*, vol. 39, pp. 527-729, 2008.

[38] M. Shojima, M. Oshima, K. Takagi, *et al*, "Magnitude and role of wall shear stress on cerebral aneurysm: computational fluid dynamic study of 20 middle cerebral artery aneurysms," *Stroke*, vol. 35, pp. 2500-2505, 2004.

[39] A. M. Malek, S. L. Alper, and S. Izumo, "Hemodynamic shear stress and its role in atherosclerosis," *JAMA*, vol. 282, pp. 2035-2042, 1999.

Table 1. Material parameters of an intracranial aneurysm.

Material Parameters	**C_{10} (MPa)**	**C_{01} (MPa)**	**C_{11} (MPa)**	**C_{20} (MPa)**	**C_{02} (MPa)**
Aneurysm	0.024	0.026	0.42	—	—
Parent Artery	0.05045	0.03049	0.12	0.4	0.01

FIGURE CAPTIONS

Fig. 1 Definitions of important components of a flow diverter.

Fig. 2 (a) Hybrid flow diverter design and (b) lighter side (left) and denser side (right) facing an aneurysm.

Fig. 3 (a) Intracranial aneurysm model and (b) the flow property: relation between dynamic viscosity and shear strain rate for the Carreau–Yasuda Model.

Fig. 4 The blood flow model of an intracranial aneurysm after the hybrid flow diverter deployment: (a) front view, (b) top view, and (c) its average inlet flow velocity of intranial aneurysm.

Fig. 5 (a) Surface monitor of inflow rate, (b) inflow ratio of surface monitor and inlet boundary before deployment of the hybrid blood diverter, and (c) deployment of the hybrid flow diverter.

Fig. 6 Contour plots of strain distribution for the hybrid flow diverter (a) expansion and (b) crimping during manufacturing simulation, (c) Goodman diagram of the hybrid flow diverter, and (d) Comparison of metal densities for the lighter side (top) and the denser side (bottom) of the hybrid flow diverter after expansion.

Fig. 7 (a) Comparison of the inflow rate before and after deployment and (b) inflow reduction rate after deployment of the hybrid flow diverter.

Fig. 8 (a) Comparison of the residence time before and after deployment and (b) increasing rate of residence after deployment of the hybrid flow diverter.

Fig.9 (a) Contour plots of streamline before (left) and after (right) deployment and (b) Partial enlargement of streamline before (left) and after (right) deployment of the hybrid flow diverter.

Fig. 10 (a) Central section of the flow velocity contour before (left) and after (right) deployment and (b) partial enlargement of the flow velocity contour before (left) and after (right) deployment of the hybrid flow diverter.

Fig. 11 (a) Contour plots of wall shear stress distribution before (left) and after (right) deployment and (b) partial enlargement of wall shear stress distribution before (left) and after (right) deployment of the hybrid flow diverter.

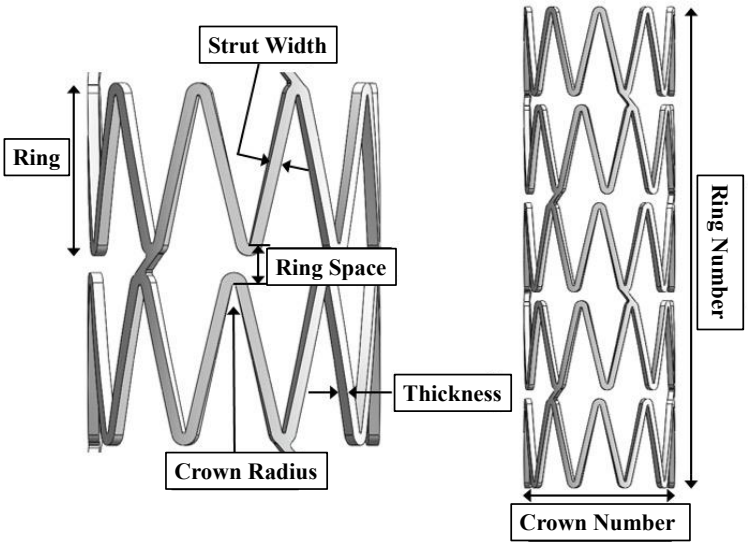

Fig. 1 Definitions of important components of a flow diverter.

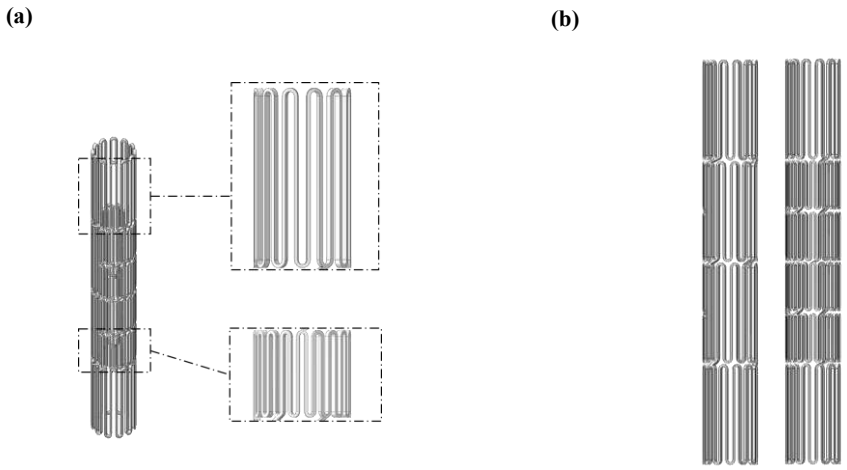

Fig. 2 (a) Hybrid flow diverter design and (b) lighter side (left) and denser side (right) facing an aneurysm.

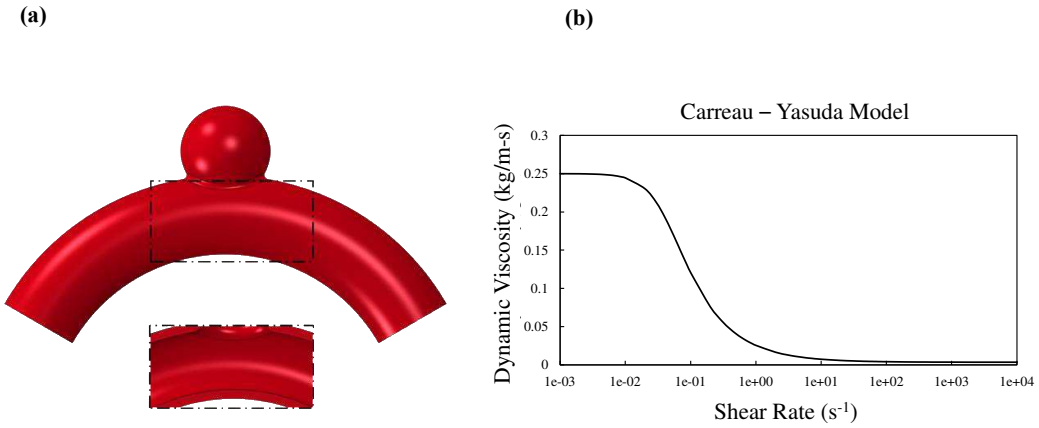

Fig. 3 (a) Intracranial aneurysm model and (b) the flow property: relation between dynamic viscosity and shear strain rate for the Carreau–Yasuda Model.

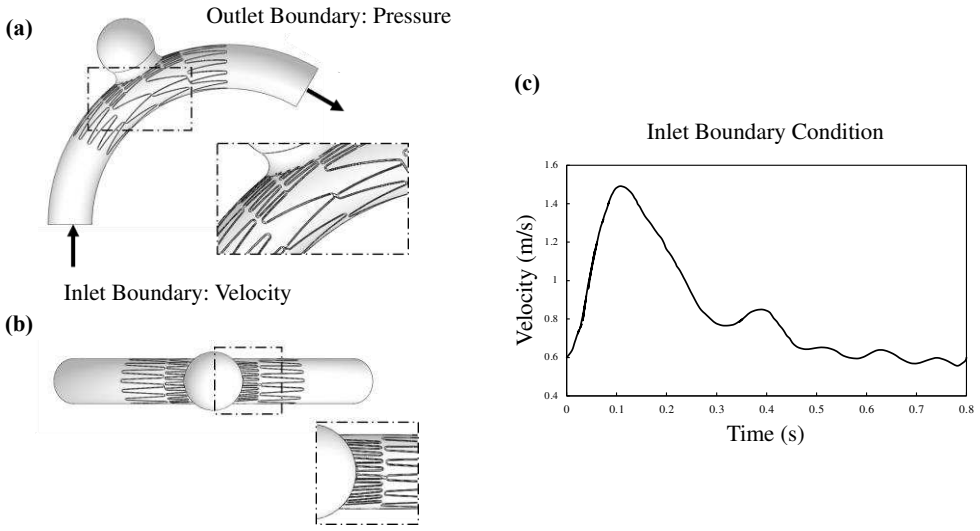

Fig. 4 The blood flow model of an intracranial aneurysm after the hybrid flow diverter deployment: (a) front view, (b) top view, and (c) its average inlet flow velocity of intranial aneurysm.

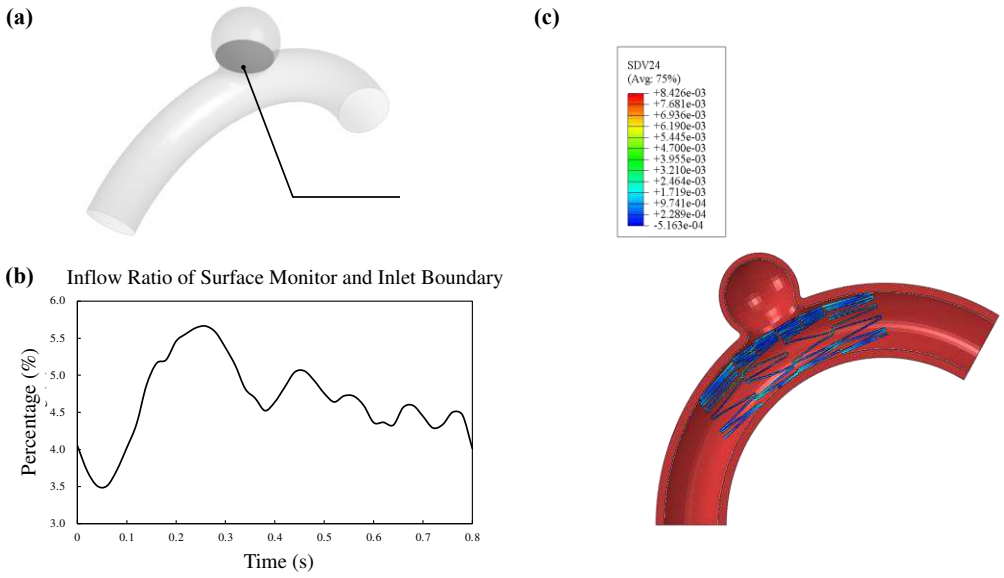

Fig. 5 (a) Surface monitor of inflow rate, (b) inflow ratio of surface monitor and inlet boundary before deployment of the hybrid blood diverter, and (c) deployment of the hybrid flow diverter.

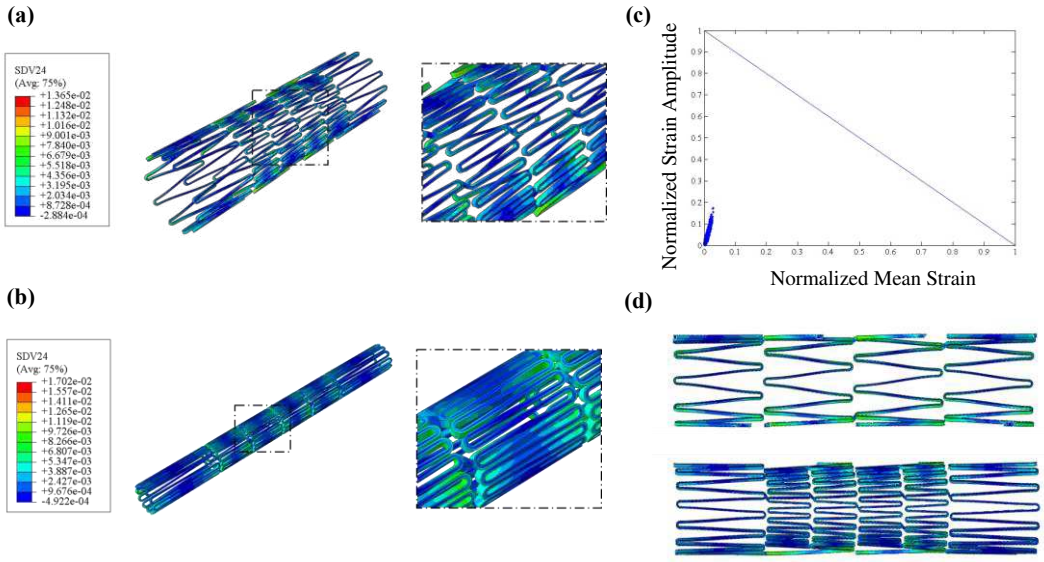

Fig. 6 Contour plots of strain distribution for the hybrid flow diverter (a) expansion and (b) crimping during manufacturing simulation, (c) Goodman diagram of the hybrid flow diverter, and (d) Comparison of metal densities for the lighter side (top) and the denser side (bottom) of the hybrid flow diverter after expansion.

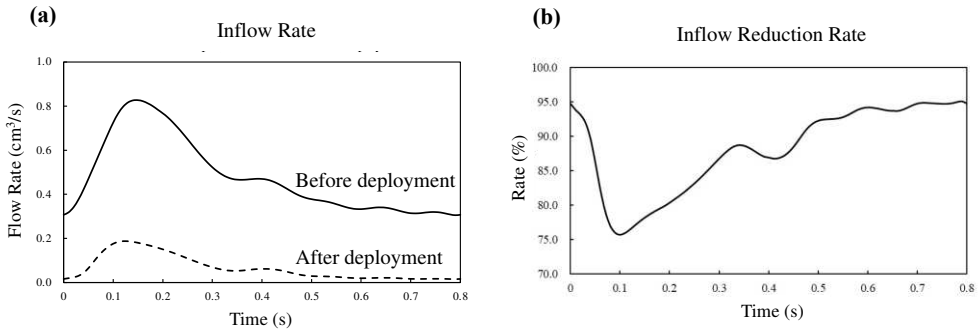

Fig. 7 (a) Comparison of the inflow rate before and after deployment and (b) inflow reduction rate after deployment of the hybrid flow diverter.

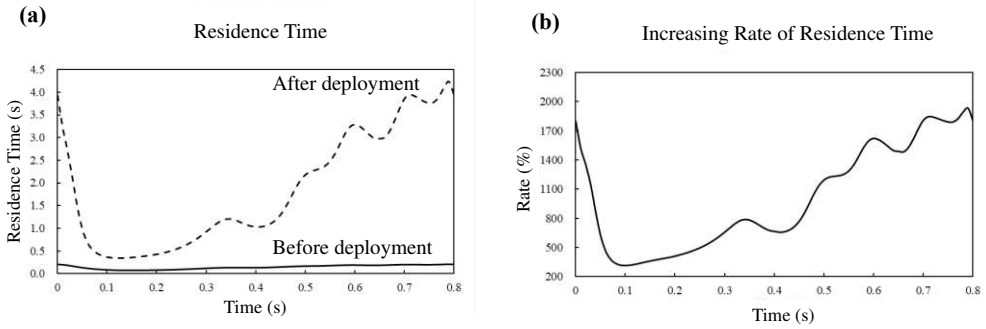

Fig. 8 (a) Comparison of the residence time before and after deployment and (b) increasing rate of residence after deployment of the hybrid flow diverter.

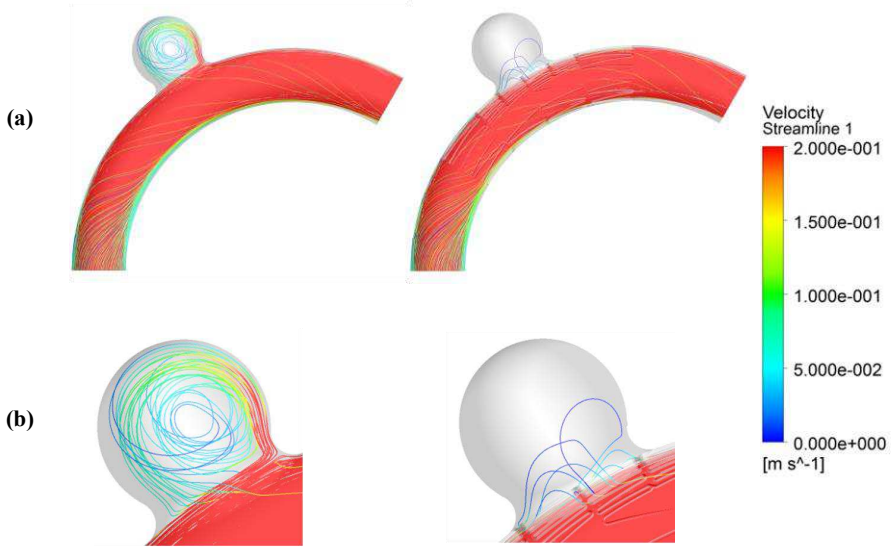

Fig.9 (a) Contour plots of streamline before (left) and after (right) deployment and (b) Partial enlargement of streamline before (left) and after (right) deployment of the hybrid flow diverter.

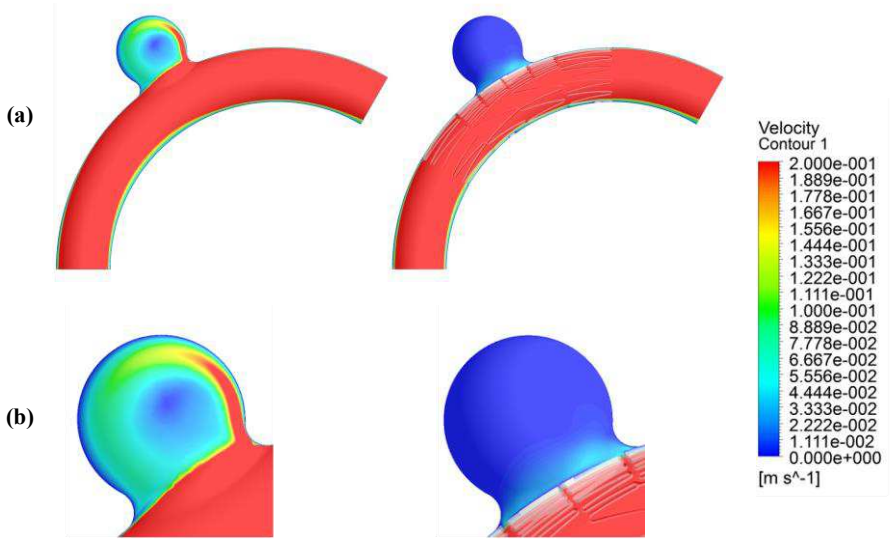

Fig. 10 (a) Central section of the flow velocity contour before (left) and after (right) deployment and (b) partial enlargement of the flow velocity contour before (left) and after (right) deployment of the hybrid flow diverter.

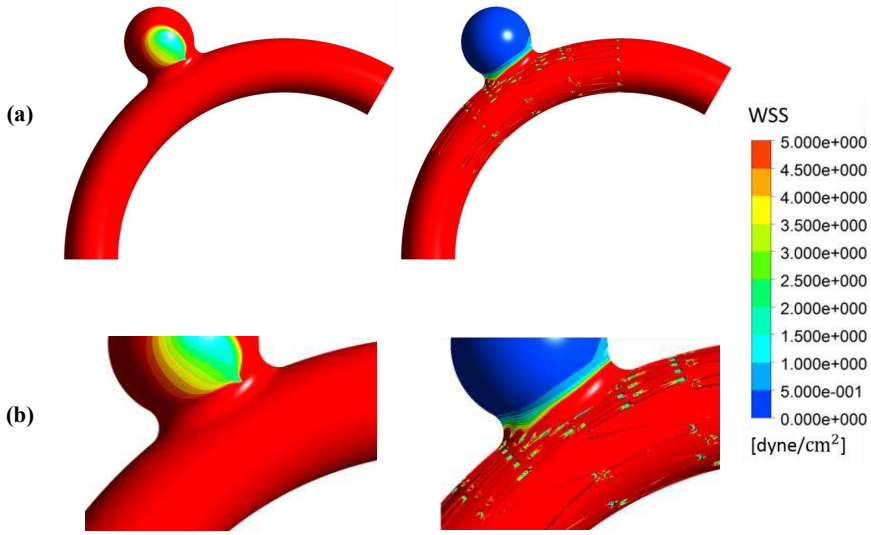

Fig. 11 (a) Contour plots of wall shear stress distribution before (left) and after (right) deployment and (b) partial enlargement of wall shear stress distribution before (left) and after (right) deployment of the hybrid flow diverter.